Anomalous entropic effect on catalysis via surface pre-melting of nanoclusters revealed by machine-learning molecular dynamics

Fu-Qiang Gong,[†] Yun-Pei Liu,[†] Ye Wang,[†] Weinan E,[‡,¶] Zhongqun Tian,[†,§] and Jun Cheng*[*,†,§,‖]

[†]*State Key Laboratory of Physical Chemistry of Solid Surface, iChEM, College of Chemistry and Chemical Engineering, Xiamen University, Xiamen, 361005, China*

[‡]*Center for Machine Learning Research, School of Mathematical Sciences, Peking University, Beijing, 100084, China*

[¶]*AI for Science Institute, Beijing, 100080, China*

[§]*Laboratory of AI for Electrochemistry (AI4EC), IKKEM, Xiamen, 361005, China*

[‖]*Institute of Artificial Intelligence, Xiamen University, Xiamen, 361005, China*

Received October 25, 2023; E-mail: chengjun@xmu.edu.cn

Abstract: Due to the superior catalytic activity and efficient utilization of noble metals, nanocatalysts are extensively used in the modern industrial production of chemicals. The surface structures of these materials are significantly influenced by reactive adsorbates, leading to dynamic behavior under experimental conditions. The dynamic nature poses significant challenges in studying the structure-activity relations of catalysts. Herein, we unveil an anomalous entropic effect on catalysis via surface pre-melting of nanoclusters through machine learning accelerated molecular dynamics and free energy calculation. We find that due to the pre-melting of shell atoms, there exits a nonlinear variation in the catalytic activity of the nanoclusters with temperature. Consequently, two notable changes in catalyst activity occur at the respective temperatures of melting for the shell and core atoms. We further study the nanoclusters with surface point defects, i.e. vacancy and ad-atom, and observe significant decrease in the surface melting temperatures of the nanoclusters, enabling the reaction to take place under more favorable and milder conditions. These findings not only provide novel insights into dynamic catalysis of nanoclusters but also offer new understanding of the role of point defects in catalytic processes.

■ INTRODUCTION

Since the early 1900s, when Wilhelm Ostwald first coined the term "catalyst",[1] these materials have garnered extensive attention due to their remarkable ability to effectively change the rate of chemical reactions and facilitates the synthesis of chemicals with higher conversion yields. With the development of *in situ* and *operando* characterization techniques,[2–4] numerous studies have shown that the structures, morphologies, and even compositions of catalysts can exhibit significant variations at different states under reaction conditions, particularly for their surfaces,[5–12] where catalytic reactions primarily occur. Unfortunately, the atomic-scale picture of catalytic processes remains largely unclear due to limitations of characterization techniques in spatial and temporal resolution.[13]

On the other hand, computational approaches can provide a useful tool for investigating structural dynamics of catalysts and its role in catalysis at the atomic level.[14? –16] For instance, Sun et al.[17] have applied *ab initio* molecular dynamics (AIMD) to investigate dynamic structures of sub-nanometer clusters and further calculated reaction energies and barriers on some meta-stable isomers using static structure optimization.[18] These studies have highlighted the significance of meta-stable isomers of catalysts in affecting the activity, and however this approach still relies on preselected isomeric structures for studying elementary reactions. Clearly, an ensemble representation of catalyst structures that takes into account all relevant configurations contributing to reaction free energies, is only adequate to accurately portray the full, statistic nature on catalyst dynamics.[18] Recently, Cheng and coworkers[19–22] have combined AIMD and enhanced sampling methods to rigorously calculate reaction free energies on dynamical sub-nanometer metal clusters at varying temperatures, and found that the small clusters can undergo phase transitions owing to strong coupling with surface intermediates during elementary reactions, facilitating the reactions.[23–25] However, in many catalytic processes, the catalysts typically fall in several to tens of nanometer size, and it seems unlikely that surface species would significantly affect the dynamics of the whole nanoparticles, suggesting limited impact on reactivity. While, surfaces may play an important role in structural dynamics, and thus the interesting question to ask is how surface dynamics affects the activity in nanosized catalysts.

We present here our study on dynamic catalysis on nanoclusters, enabled by machine learning accelerated molecular dynamics (MLMD), surpassing the limitations of AIMD on spatial and time scale. Specifically, we investigate CO_2 dissociation (reverse of CO oxidation) reaction catalyzed by three copper nanoclusters, i.e. Cu_{54}, Cu_{55}, and Cu_{56}, at different temperatures. Notably, the Cu_{55} cluster exhibits a highly symmetrical icosahedral structure,[26,27] while Cu_{54} and Cu_{56} can be considered as Cu_{55} with a vacancy and an ad-atom, respectively. This selection of model systems enables us to study the influence of point defects on surface dynamics of the catalysts, as illustrated in Figure. 1. Interestingly, our calculation discovers that these nanoclusters show a surface pre-melting behavior during the catalytic reaction, which give rise to anomalous entropy changes and has great impact on the catalytic activity. Moreover, our results show that point defects like vacancies and ad-atoms, can lead to increased dynamics of the surface structures of the nanoclusters, thereby facilitating reactions under milder conditions. We expect that our work opens up a new angle to understand catalyst dynamics and helps develop new strategies to optimize catalytic performances.

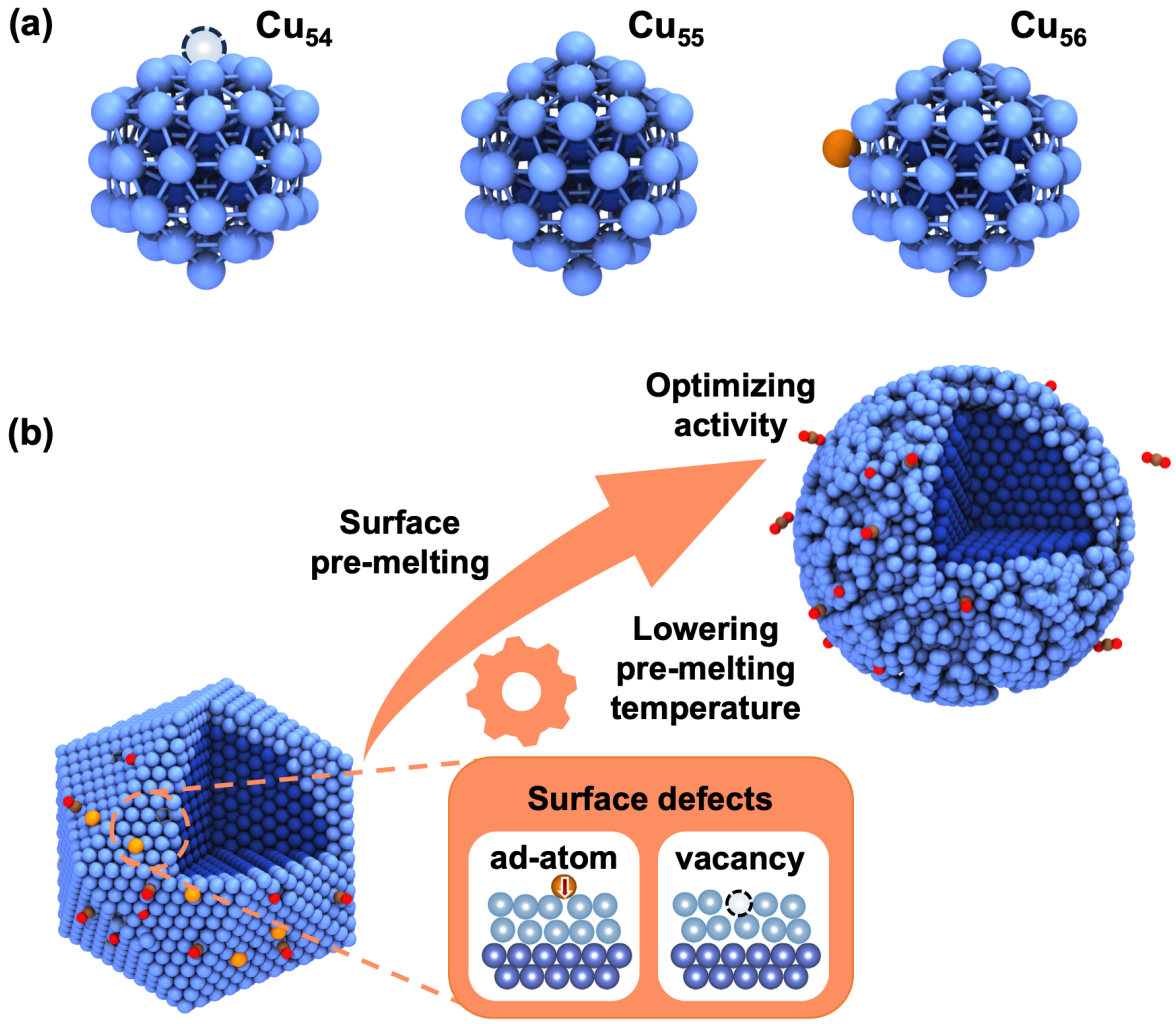

Figure 1. **(a)** Model systems to investigate the surface dynamics of nanoclusters, namely Cu_{54} (upper), Cu_{55} (middle), and Cu_{56} (bottom), where the dark blue, light blue, transparent and orange balls represent the core, shell atoms, surface vacancy, and ad-atom, respectively; **(b)** Schematic illustration on how surface vacancy and ad-atom affect surface dynamics and catalytic activity of nanoclusters, where the grey, and red balls indicate the carbon and oxygen atoms, respectively.

■ METHODS SECTION

DFT setup. All DFT calculations are carried out by freely available program package – CP2K/QUICKSTEP.[28,29] The core electrons are described by Goedecker-Teter-Hutter (GTH) type pseudopotentials.[30] The electronic exchange and correlation energies are described by Perdew-Burke-Ernzerhof (PBE) functional[31] with the Grimme D3 dispersion correction.[32] The valence electrons of Cu, C and O atoms are Gaussian-type triple ζ basis with two polarization function (TZV2P),[33] and an auxiliary plane wave basis with an 800 Ry cutoff is used to re-expand the electron density.[34] The orbital transformation (OT) algorithm[35] is used to optimize self-consistent wavefunction (SCF) when the charge density residual converges to 1.0×10^{-6} a.u..

Workflow of MLP construction. To construct the MLP for investigating the structural dynamics of nanocatalysts during the reaction, we employ a concurrent learning strategy combine with Well-Tempered MetaDynamics (WT-MetaD). The workflow contains three main components: training, exploration and labeling. These three steps are repeated iteratively until the final MLPs are accurate enough for atomic simulation which are implemented in Deep Potential GENerator (DP-GEN) package.[36] Here is a brief description of the workflow:

a). To initiate the training step of workflow, initial datasets are needed, in which case we collect 200 structures and corresponding energies and atomic forces through AIMD combined with WT-MetaD.

b). Training: An end-to-end symmetry preserving interatomic potential energy model, Deep Potential – Smooth Edition (DeepPot-SE),[37] is used to construct the potential energy surface (PES). Four DeepPot-SE models are constructed based on the same training data but with different random seeds through freely available package DeePMD-kit,[38] so all these models can fit the datasets but have different model parameters. For training parameters, the local environment is constructed with cutoff and smooth cutoff set to be 15 Å and 2 Å, and the embedding, fitting neuron net and axis neuron are set to be {25 50 100}, {240 240 240} and 16, respectively.

c). Exploration: Through one of the four models, we employ WT-MetaD to enhance MD sampling so that the dissociation of CO_2 on Cu nanocluster can occur during the simulation. The maximum force deviation (see ref[36] for more detailed information) among four models is calculated as a criterion to select the new structures with moderate values ($0.2 - 0.4$ eV/ Å). In each iteration, several enhanced MD simulations are conducted at 50-1600 K.

d). Labeling: The new structures from exploration are labeled with DFT calculation according to the same setup as AIMD and added into the training datasets, so a better MLP can be obtained.

In order to construct the MLP for free energy calculation of CO_2 dissociation on Cu_{54}, Cu_{55} and Cu_{56} nanoclusters, 4250 frames of $Cu_{54}CO_2$ and 2600 frames of $Cu_{56}CO_2$ are collected as training datasets. Additionally, we have also validated its accuracy on the $Cu_{55}CO_2$ system, as discussed in SI.

Free energy calculation. Our study combined WT-MetaD with MLMD to obtain free energy profiles for CO_2 dissociation at different temperatures. The reaction coordinate was chosen as the distance between the carbon and oxygen atoms. The MD simulations were performed in the NVT ensemble using a velocity rescaling thermostat (CSVR) with a time step of 0.5 fs.[39] WT-MetaD,[40] introduces a time-dependent bias Gaussian potential along the reaction coordinate, enabling enhanced sampling of rare events in molecular simulations. By biasing the system away from previously sampled regions of configuration space, WT-MetaD allows the reconstruction of the free energy surface (FES) as a function of the chosen reaction coordinates. Each simulation was carried out for 20-50 nanoseconds to ensure convergence, and detailed parameters for WT-MetaD simulation can be found in the SI.

■ RESULTS AND DISCUSSION

Free energies of CO_2 dissociation on dynamic Cu nanocluster. Investigation of the influence of the dynamic catalyst structures on catalytic reactions poses a significant challenge for theoretical methodologies, demanding sufficient statistical sampling and *ab initio* electronic structure calculation to accurately depict bond-breaking and forming events. This challenge is even more pronounced for nanocatalysts, as the timescale required for first principle calculation increases significantly with the size of the system,[41] which makes the study of nanometer systems using traditional AIMD computationally prohibitive. In this work, we combine concurrent learning scheme[36] and enhanced sampling method[42] to train a MLP for Cu nanoclusters catalyzing CO_2 dissociation, and rigorously validate the accuracy for the studied systems, as demonstrated in the Figure. S1-3 of Supporting Information (SI). With this MLP, we are able to calculate reaction free energies on nanocatalysts with sufficient statistical sampling and significantly reduced computational cost, while maintaining *ab initio* accuracy.

The free energy profiles of CO_2 dissociation catalyzed by Cu_{55} at various temperatures are obtained by Well-Tempered MetaDynamics (WT-MetaD)[40] (see Methods, SI), as shown in Figure. 2**(a)**. To verify the statistical convergence, We have computed the free energy barriers ($\Delta G^{\neq}$) and reaction free energies ($\Delta_r G$) as a function of sampling time (see Figure. S5). The convergence of free energy differences can be achieved in tens of nanoseconds of MLMD simulations, well beyond the timescale of tens of picoseconds affordable by AIMD. Based on the temperature dependence of $\Delta G^{\neq}$ and $\Delta_r G$ illustrated in Figure. 2**(b)**, it can be observed that both gradually increase as the temperature rises. Surprisingly, there are two abrupt jumps in both curves around 650 K and 850 K, suggesting significant changes in the catalyst's activity within these temperature ranges. The corresponding values at different temperatures are presented in Table S3. The non-linear variation of $\Delta G^{\neq}/\Delta_r G$ as a function of temperature has also been observed in the catalysis of sub-nanometer clusters, which was attributed to the entropic effects owing to phase transitions in subnanocatalyst.[19–22] Thus, in the following we carry out detailed analyses on the entropic effect of structural dynamics and possible phase transitions of nanoclusters to elucidate the underlying mechanism causing the two sudden changes in free energies.

Entropic effect on catalysis via surface pre-melting of metal nanoclusters. By taking a derivative of free energy differences with respect to temperature,[43] the activation entropy ($\Delta S^{\neq}$) and reaction entropy ($\Delta_r S$) are obtained

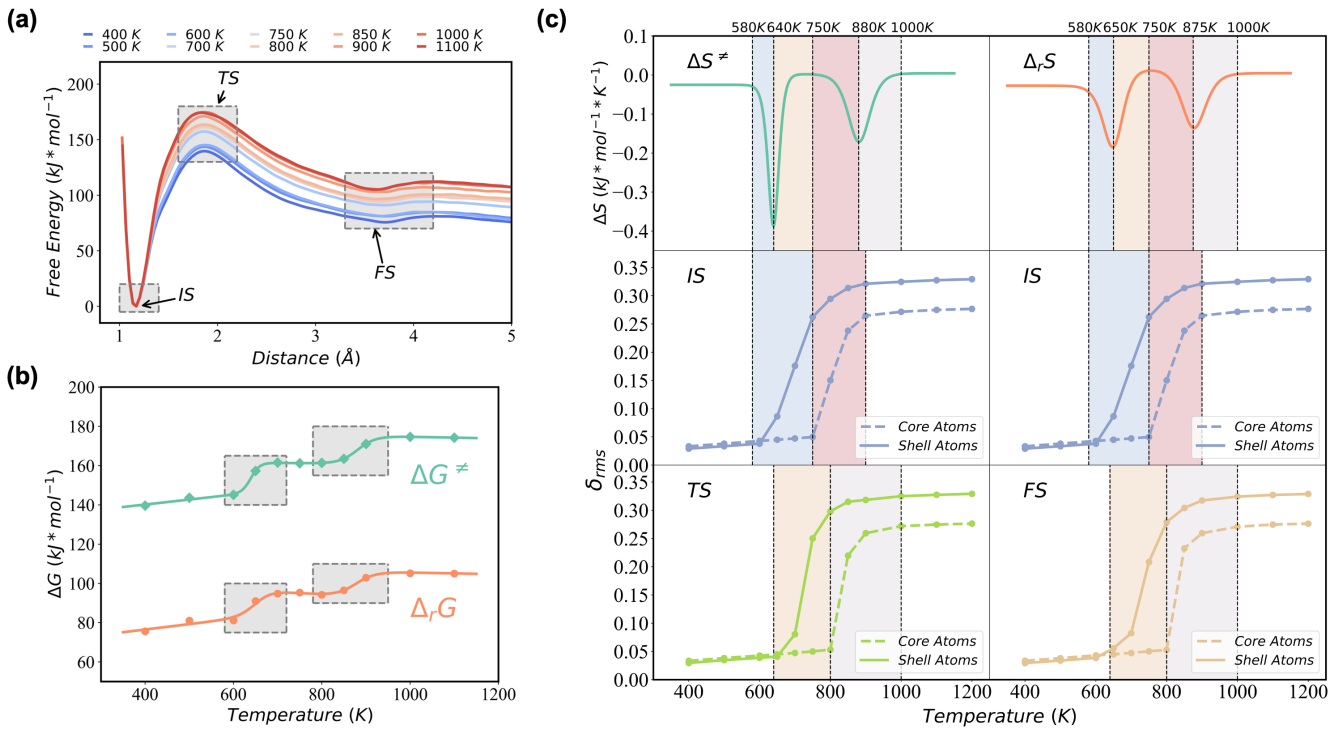

Figure 2. **(a)** The free energy curves of Cu_{55} catalyzing CO_2 dissociation reaction at different temperatures; **(b)** The free energy barriers ($\Delta G^{\neq}$) and reaction free energies ($\Delta_r G$) as a function of temperature; **(c)** The entropy changes and Lindeman index (δ_{rms}) as a function of temperature. Left panel: The activation entropy ($\Delta S^{\neq}$) and δ_{rms} of initial state (IS) and transition state (TS) for shell atoms (solid line) and core atoms (dashed line); Right panel: The reaction entropy ($\Delta_r S$) and δ_{rms} of IS and final state (FS).

as shown in the upper panel of Figure. 2**(c)**. Both $\Delta S^{\neq}$ and $\Delta_r S$ exhibit two negative peaks at the temperatures where the free energy differences change dramatically, indicating that the differences of the entropies between initial state (IS) and transition/final state (TS/FS) increase significantly at these temperatures. Further, we investigate the temperature dependence of structural dynamics of nanoclusters at IS, TS, and FS by computing the Lindemann index (δ_{rms})[44] (Methods section in SI). δ_{rms} serves to measure the extent of atomic motion in nanosized systems,[45] and small and large values correspond to solid-like and liquid-like states, respectively. Additionally, to identify which atoms become more dynamic than others, we calculate the atomic Lindemann index ($\delta_{rms,atomic}$) and present the results in Figure. S10. Interestingly, at 650 to 800 K, atoms located further from the center of mass of the Cu_{55} exhibit enhanced dynamical behavior. Accordingly, we classify the atoms in the nanocluster into core and shell atoms based on their distances from the center of mass. For Cu_{55} atoms within 3 of the center of mass can be considered as core atoms, while the rest near the surface are shell atoms. The melting behaviors of shell and core atoms at IS, TS, and FS are illustrated as S-shaped T-δ_{rms} curves and compared in the middle and bottom panel of Figure. 2**(c)**. Evidently, the melting temperatures of the shell atoms are about 200 K lower than those of the core atoms, indicating a pre-melting behavior of the nanocatalyst, which is similar to previous findings.[46–48]

The intriguing observation arises from the different melting temperatures among different reaction states for both core atoms and shell atoms. At temperatures below ~600 K or above ~900 K, both the shell and core atoms of the different reaction states are either in solid-like or liquid-like states, respectively (the white regions in the middle and bottom panel of Figure. 2**(c)**). Thus, the entropy differences between IS and TS/FS, i.e., $\Delta S^{\neq}$ and $\Delta_r S$, are relatively small (the white regions in the upper panel of Figure. 2**(c)**). Between ~600 K and ~650 K, the core atoms of all reaction states remain in the solid-like state. However, because the shell atoms of the IS become more dynamic than those of the TS/FS (the blue regions in the middle panel of Figure. 2**(c)**), the entropy contribution from the shell atoms of the IS increases, leading to a decrease in $\Delta S^{\neq}/\Delta_r S$ (the blue regions in the upper panel of Figure. 2**(c)**). After ~650 K, the shell atoms of TS/FS become more dynamical (the yellow regions in the bottom panel of Figure. 2**(c)**), and the increase in entropy of these two states compensates for the entropy increase of the surface atoms of IS, resulting in an increase in $\Delta S^{\neq}/\Delta_r S$ (the yellow regions in the upper panel of Figure. 2**(c)**). The similar mechanism can also be applied to the temperature range of ~800 and ~900 K, in which the core atoms of different states melt at different temperature ranges (the pink and gray regions in the Figure. 2**(c)**), inducing negative peaks of $\Delta S^{\neq}/\Delta_r S$.

The negative peaks of entropy suggest that CO_2 dissociation reaction are more likely to happen at lower temperatures. More importantly, the reverse reaction, i.e., CO oxidation, can be facilitated through pre-melting and core-melting of nanoclusters. It should be emphasized that the surface pre-melting is likely to be commonly present in many nanocatalytic systems under realistic catalytic conditions, as evidenced not only by theoretical investigations[46] but also by observations using *in situ* characterization techniques.[47] Additionally, many experimental studies have provided evidence that the surface structure of the catalysts undergoes dynamic changes during catalytic reactions.[49,50] However, despite these observations, a comprehensive correlation be-

tween the dynamics of surface structure and catalytic activity has not been established. In this regard, we have demonstrated for the first time that the activity of catalysts can be altered by the surface pre-melting mechanism, specifically through the entropy contributions originating from the surface atoms. In contrast to sub-nanometer clusters, it is possible to achieve phase transition catalysis in nanoclusters at relatively lower temperatures due to the strong interaction between the reactant molecules and the surface atoms.

Surface dynamics of metal nanoclusters enhanced by point defects. In real catalytic systems, defects are often present on the catalyst surfaces, and their vital role in the catalytic reactions has been extensively studied and confirmed in recent years.[51–53] Understanding the influence of these defects on the surface dynamics of catalysts and their subsequent impact on catalyst activity is crucial for the rational design of catalysts with improved performance. Therefore, we further investigate CO_2 dissociation reaction on Cu_{54} and Cu_{56} clusters, which can be considered as highly symmetric Cu_{55} containing point defects in the form of vacancy and ad-atom, respectively.

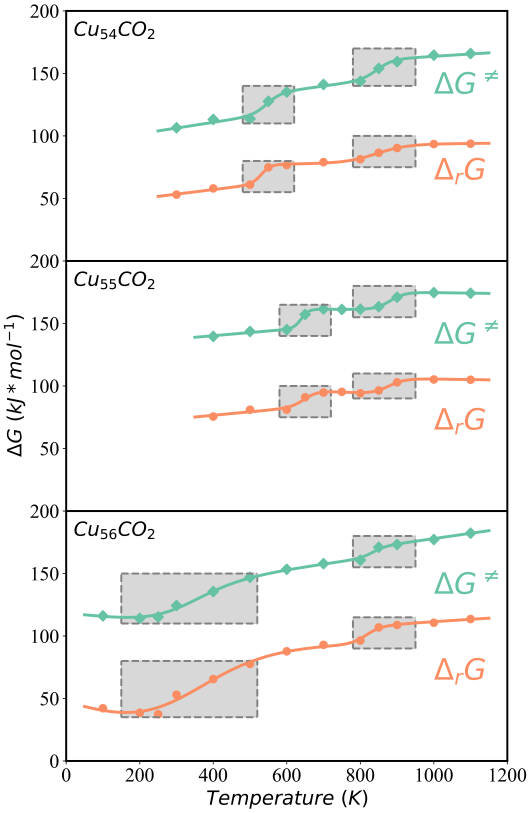

Figure 3. Temperature dependence of free energy barriers ($\Delta G^{\neq}$, green lines) and reaction free energies ($\Delta_r G$, orange lines) for CO_2 dissociation on Cu_{54} (upper panel), Cu_{55} (middle panel) and Cu_{56} (lower panel)

The free energy profiles of Cu_{54} and Cu_{56} catalyzing CO_2 dissociation as a function of temperature are calculated and presented in Figure. S7**(a)** and 8**(a)**, and the time accumulative averages of the corresponding $\Delta G^{\neq}$ and $\Delta_r G$ to check the statistical convergence are displayed in Figure. S4 and S6, respectively. The $\Delta G^{\neq}/\Delta_r G$ on the three Cu_{54}, Cu_{55} and Cu_{56} nanclusters are compared and plotted as a function of temperature in Figure. 3, and the detailed values can be found in Table S2 and S4. Similar to Cu_{55}, the temperature dependent $\Delta G^{\neq}/\Delta_r G$ curves for Cu_{54} and Cu_{56} also exhibit two distinct jumps, which can be attributed to differences in the melting temperatures of the shell and core atoms between IS and TS/FS, as illustrated in Figure. S7**(c)** and S8**(c)**.

It is commonly accepted that the presence of surface defects, i.e. vacancies and ad-atoms, can affect the activity due to lower coordination numbers of surface atoms and higher adsorption energies, as illustrated in Figure. S12 and S13. On the other hand, what we find most intriguing here is that the temperatures at which free energies change significantly differ among these three nanoclusters, especially for the first transitions (see Figure. 3). According to detailed analyses of the melting behaviors of these three nanoclusters (Figure. 4**(a)**,**(b)** and Figure. S14), the observed differences in first transition temperatures of ΔG can be attributed to changes in the onset melting temperatures of shell atoms. Specifically, the melting temperatures of shell atoms for Cu_{54}, Cu_{55}, and Cu_{56} are 550, 650, and 150 K, respectively. This finding indicates that point defects, such as vacancies and ad-atoms, can lower the pre-melting temperature of Cu_{55} nanocluster, thus affecting reactivity. Since the core atoms exhibit similar melting temperatures, the temperatures corresponding to the second transitions in free energies are very similar.

On Cu_{54} there is a vacancy on the surface, which provides a free site for the neighboring atoms and make them more dynamic, and the nanocluster has a lower pre-melting temperature of the shell atoms than Cu_{55}. This is supported by comparing the probability distributions of copper atoms relative to the centers of mass of the two nanoclusters ($P(r)$) obtained from MD simulations at 600 K, a temperature at which the shell atoms of Cu_{54} start to melt while the shell atoms of Cu_{55} remain solid-like. The presence of a vacancy on the surface facilitates more frequent atomic exchanges between the corner and edge atoms of the first shell (the blue area in Figure. 4**(c)**). Moreover, the vacancy may even allow core atoms to switch positions with those from the surface region (the inset figure of Figure. 4**(c)**), thereby resulting in a non-zero value of $P(r)$ between the core and shell region, in contrast to Cu_{55} in which similar atomic exchange is not observed. As for Cu_{56}, it is remarkable that the surface melting temperature is about 400 K lower than that of Cu_{55}, which can be attributed to the presence of an ad-atom on the surface. Below ∼150K, the ad-atom is identified as the peak more than 5 away from the center of mass of the nanocluster, as indicated by the pink circle in Figure. 4**(d)** and Figure. S11. When the temperature is above 150 K, this peak is reduced and broadened, and $P(r)$ exhibits non-zero values within the range of 4.8 to 5.6 (see the inset of Figure. 4**(d)**)), in contrast to the distribution at 100 K, indicating that the ad-atom can penetrate into the surface. The penetration of the ad-atom can significantly alter the arrangement of the surface atoms at 150 K and induce dynamic exchange of shell atoms comparing to those at 100 K (the blue area in Figure. 4**(d)**). Thus, the surface melting temperature can be significantly lowered in the presence of the ad-atom.

By comparing the symmetrical nanocluster Cu_{55} and the clusters with one atom more or less, the surface point defects, i.e. vacancies and ad-atoms, have been revealed to significantly impact surface dynamics and lower the pre-melting temperatures of nanocatalysts. Thus, our MLMD calculations clearly demonstrate that the commonly present point defects on the surfaces of nanocatalysts can facilitate surface reactions at lower temperatures by a significant en-

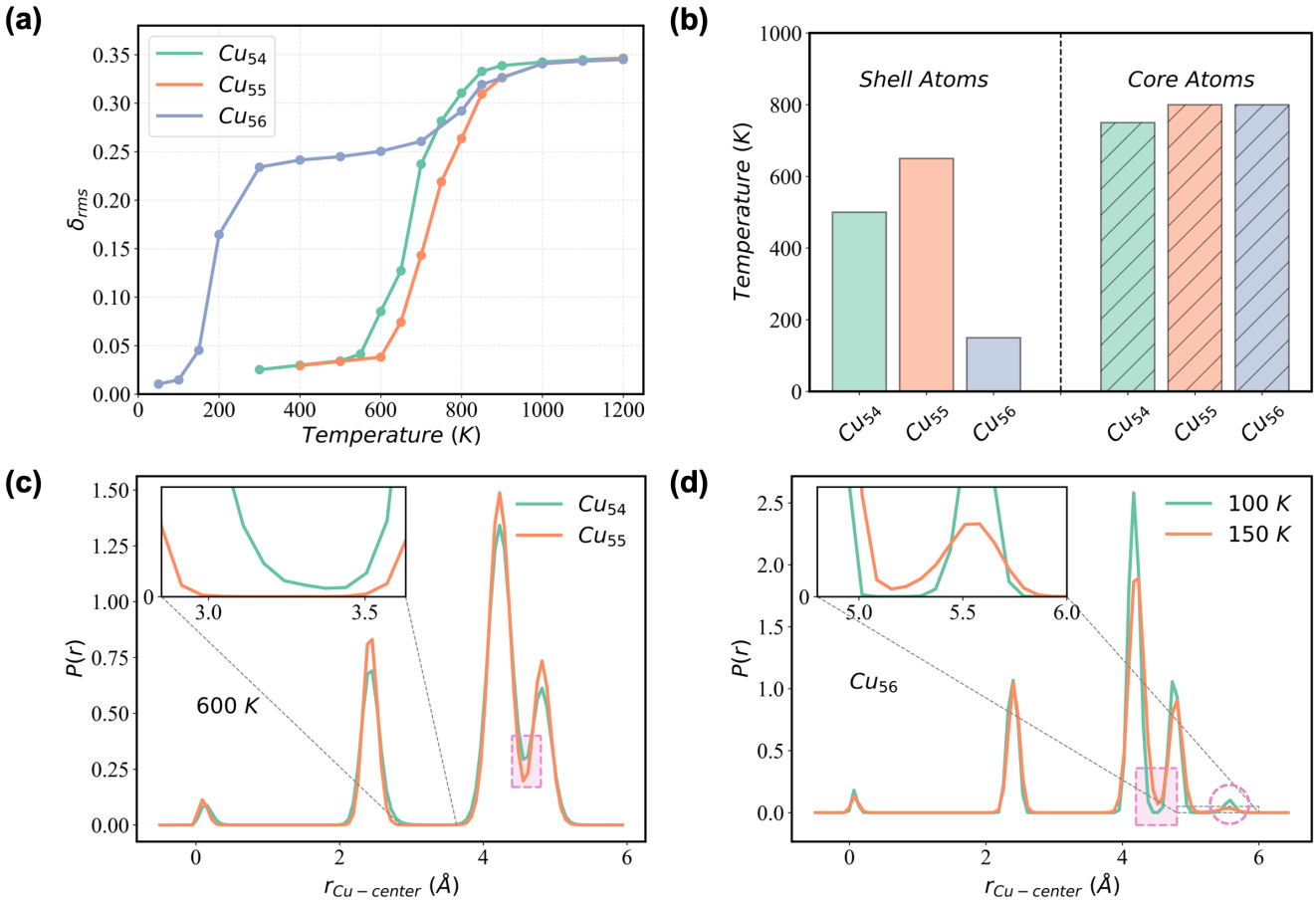

Figure 4. **(a)** The calculated δ_{rms} as a function of temperature, with the green, purple, and orange lines corresponding to Cu_{54}, Cu_{55}, and Cu_{56}, respectively; **(b)** The onset temperatures of phase transitions for shell (left) and core atoms (right) of different nanoclusters; **(c)** The probability distribution functions of the copper atoms relative to the center of mass of the cluster ($P(r)$) based on the MD simulations for Cu_{54} and Cu_{55} at 600 K; **(d)** The $P(r)$ for Cu_{56} at 100 and 150 K.

tropic factor induced by the surface pre-melting behaviour.

■ CONCLUSION

It is likely that this theoretically discovered abnormal entropy effect induced by the surface pre-melting may be widely present in many catalytic systems involving nanocatalysts without being realized. In literature, many studies have observed structural dynamics of surface atoms of catalysts under environmental conditions, which is suggested to correlate with the changes in catalytic activity. For instance, it has been found that the oscillatory change in the activity of CO oxidation is attributed to the order-disorder transformation of the surface of Pt nanocatalysts.[54,55] Similarly, the formation of a dynamical self-hydrogenated shell on the surface of TiO_2 has been observed by using transmission electron microscopy and is believed to enhance photocatalytic hydrogen evolution reaction.[56] Furthermore, our finding suggests a new mechanism to improve catalyst performances by engineering surface defects to tune surface dynamics and pre-melting behavior. We expect that the development of catalyst synthetic methods such as wet chemical method[57] and gradient assembly method,[58] may enable precise control over catalyst size, potentially leading to defect-induced phase transition catalysis of dynamic nanoclusters.

To sum up, we combine enhanced sampling and concurrent learning methods to obtain accurate machine learning potentials to calculate free energies of dynamic catalysis on nanoclusters. We discover a new surface pre-melting mechanism that can significantly change free energies of surface reactions due to anomalous entropic effect associated with strong coupling of reaction intermediates and surface atoms.Furthermore, we find that surface vacancy and adatom can alter the surface dynamics and thus catalytic activity by lowering the pre-melting temperature, with the former offering free site to neighboring surface atoms to move around, and the latter penetrating into and significantly perturbing the surface structure. Therefore, our work provides new insights into dynamic catalysis and the role of surface defects in catalysis, which may help develop strategies of engineering surface defects and dynamics to improve catalysts.

Acknowledgement F.-Q. G. gratefully acknowledges Xiamen University and iChEM for a Ph.D. studentship. J.C. gratefully acknowledges funding from the National Science Fund for Distinguished Young Scholars (Grant No. 22225302), the National Natural Science Foundation of China (Grant Nos. 92161113, 21991151, 21991150, and 22021001) and the Fundamental Research Funds for the Central Universities (Grant No. 20720220008, 20720220009, 20720220010), Laboratory of AI for Electrochemistry (AI4EC), and IKKEM (Grant Nos. RD2023100101 and RD2022070501).

Supporting Information Available

Details on free energy calculation method and other analysis methods; Figure S1 to S14; Table S1 to S4.

References

(1) Wilhelm, O. Catalysis. *Phys. Z* **1901**, *3*, 313–322.
(2) Hansen, T. W.; Wagner, J. B.; Hansen, P. L.; Dahl, S.; Topsøe, H.; Jacobsen, C. J. Atomic-resolution in situ transmission electron microscopy of a promoter of a heterogeneous catalyst. *science* **2001**, *294*, 1508–1510.
(3) Tao, F. F.; Crozier, P. A. Atomic-scale observations of catalyst structures under reaction conditions and during catalysis. *Chemical reviews* **2016**, *116*, 3487–3539.
(4) Liang, X.; Fu, N.; Yao, S.; Li, Z.; Li, Y. The progress and outlook of metal single-atom-site catalysis. *Journal of the American Chemical Society* **2022**, *144*, 18155–18174.
(5) Hansen, P. L.; Wagner, J. B.; Helveg, S.; Rostrup-Nielsen, J. R.; Clausen, B. S.; Topsøe, H. Atom-resolved imaging of dynamic shape changes in supported copper nanocrystals. *Science* **2002**, *295*, 2053–2055.
(6) Hrbek, J.; Hoffmann, F. M.; Park, J. B.; Liu, P.; Stacchiola, D.; Hoo, Y. S.; Ma, S.; Nambu, A.; Rodriguez, J. A.; White, M. G. Adsorbate-driven morphological changes of a gold surface at low temperatures. *Journal of the American Chemical Society* **2008**, *130*, 17272–17273.
(7) Newton, M. A. Dynamic adsorbate/reaction induced structural change of supported metal nanoparticles: heterogeneous catalysis and beyond. *Chemical Society Reviews* **2008**, *37*, 2644–2657.
(8) Yoshida, H.; Kuwauchi, Y.; Jinschek, J. R.; Sun, K.; Tanaka, S.; Kohyama, M.; Shimada, S.; Haruta, M.; Takeda, S. Visualizing gas molecules interacting with supported nanoparticulate catalysts at reaction conditions. *Science* **2012**, *335*, 317–319.
(9) Zugic, B.; Wang, L.; Heine, C.; Zakharov, D. N.; Lechner, B. A.; Stach, E. A.; Biener, J.; Salmeron, M.; Madix, R. J.; Friend, C. M. Dynamic restructuring drives catalytic activity on nanoporous gold–silver alloy catalysts. *Nature materials* **2017**, *16*, 558–564.
(10) Grosse, P.; Gao, D.; Scholten, F.; Sinev, I.; Mistry, H.; Roldan Cuenya, B. Dynamic changes in the structure, chemical state and catalytic selectivity of Cu nanocubes during CO2 electroreduction: size and support effects. *Angewandte Chemie* **2018**, *130*, 6300–6305.
(11) Luo, L.; Chen, S.; Xu, Q.; He, Y.; Dong, Z.; Zhang, L.; Zhu, J.; Du, Y.; Yang, B.; Wang, C. Dynamic atom clusters on AuCu nanoparticle surface during CO oxidation. *Journal of the American Chemical Society* **2020**, *142*, 4022–4027.
(12) Zhu, J.; Wang, P.; Zhang, X.; Zhang, G.; Li, R.; Li, W.; Senftle, T. P.; Liu, W.; Wang, J.; Wang, Y.; others Dynamic structural evolution of iron catalysts involving competitive oxidation and carburization during CO2 hydrogenation. *Science Advances* **2022**, *8*, eabm3629.
(13) Zhu, Y.; Wang, J.; Chu, H.; Chu, Y.-C.; Chen, H. M. In situ/operando studies for designing next-generation electrocatalysts. *ACS Energy Letters* **2020**, *5*, 1281–1291.
(14) Wang, Y.-G.; Yoon, Y.; Glezakou, V.-A.; Li, J.; Rousseau, R. The role of reducible oxide–metal cluster charge transfer in catalytic processes: new insights on the catalytic mechanism of CO oxidation on Au/TiO2 from ab initio molecular dynamics. *Journal of the American Chemical Society* **2013**, *135*, 10673–10683.
(15) Wang, Y.-G.; Mei, D.; Glezakou, V.-A.; Li, J.; Rousseau, R. Dynamic formation of single-atom catalytic active sites on ceria-supported gold nanoparticles. *Nature communications* **2015**, *6*, 6511.
(16) Lu, Y.; Wang, J.; Yu, L.; Kovarik, L.; Zhang, X.; Hoffman, A. S.; Gallo, A.; Bare, S. R.; Sokaras, D.; Kroll, T.; Xin, H.; Karim, A. M. Identification of the active complex for CO oxidation over single-atom Ir-on-MgAl2O4 catalysts. *Nature Catalysis* **2019**, *2*, 149–156.
(17) Geng, S.; Philippe, S. Metastable structures in cluster catalysis from first-principles: structural ensemble in reaction conditions and metastability triggered reactivity. *Journal of the American Chemical Society* **2018**, *140*, 2812–2820.
(18) Lavroff, R. H.; Morgan, H. W.; Zhang, Z.; Poths, P.; Alexandrova, A. N. Ensemble representation of catalytic interfaces: soloists, orchestras, and everything in-between. *Chemical science* **2022**, *13*, 8003–8016.
(19) Sun, J.-J.; Cheng, J. Solid-to-liquid phase transitions of subnanometer clusters enhance chemical transformation. *Nature communications* **2019**, *10*, 5400.
(20) Fan, Q.-Y.; Sun, J.-J.; Wang, F.; Cheng, J. Adsorption-induced liquid-to-solid phase transition of Cu clusters in catalytic dissociation of CO2. *The Journal of Physical Chemistry Letters* **2020**, *11*, 7954–7959.
(21) Fan, Q.-Y.; Liu, J.-L.; Gong, F.-Q.; Wang, Y.; Cheng, J. Structural dynamics of Ru clusters during nitrogen dissociation in ammonia synthesis. *Physical Chemistry Chemical Physics* **2022**, *24*, 10820–10825.
(22) Gong, F.-Q.; Guo, Y.-X.; Fan, Q.-Y.; Cheng, J. Dynamic catalysis of sub-nanometer metal clusters in oxygen dissociation. *Next Nanotechnology* **2023**, 100002.
(23) Fan, Q.-Y.; Wang, Y.; Cheng, J. Size-sensitive dynamic catalysis of subnanometer Cu clusters in CO2 dissociation. *The Journal of Physical Chemistry Letters* **2021**, *12*, 3891–3897.
(24) Fan, Q.-Y.; Shi, Z.-H.; Wang, Y.; Cheng, J. Charge State Dependence of Phase Transition Catalysis of Dynamic Cu Clusters in CO2 Dissociation. *The Journal of Physical Chemistry C* **2021**, *125*, 27615–27623.
(25) Sun, J.-J.; Fan, Q.-Y.; Jin, X.; Liu, J.-L.; Liu, T.-T.; Ren, B.;

Cheng, J. Size-dependent phase transitions boost catalytic activity of sub-nanometer gold clusters. *The Journal of Chemical Physics* **2022**, *156*, 144304.
(26) Whetten, R. L.; Khoury, J. T.; Alvarez, M. M.; Murthy, S.; Vezmar, I.; Wang, Z.; Stephens, P. W.; Cleveland, C. L.; Luedtke, W.; Landman, U. Nanocrystal gold molecules. *Advanced materials* **1996**, *8*, 428–433.
(27) Desireddy, A.; Kumar, S.; Guo, J.; Bolan, M. D.; Griffith, W. P.; Bigioni, T. P. Temporal stability of magic-number metal clusters: beyond the shell closing model. *Nanoscale* **2013**, *5*, 2036–2044.
(28) VandeVondele, J.; Krack, M.; Mohamed, F.; Parrinello, M.; Chassaing, T.; Hutter, J. Quickstep: Fast and accurate density functional calculations using a mixed Gaussian and plane waves approach. *Computer Physics Communications* **2005**, *167*, 103–128.
(29) Hutter, J.; Iannuzzi, M.; Schiffmann, F.; VandeVondele, J. cp2k: atomistic simulations of condensed matter systems. *Wiley Interdisciplinary Reviews: Computational Molecular Science* **2014**, *4*, 15–25.
(30) Hartwigsen, C.; Gœdecker, S.; Hutter, J. Relativistic separable dual-space Gaussian pseudopotentials from H to Rn. *Physical Review B* **1998**, *58*, 3641.
(31) Perdew, J. P.; Burke, K.; Ernzerhof, M. Generalized gradient approximation made simple. *Physical review letters* **1996**, *77*, 3865.
(32) Grimme, S.; Antony, J.; Ehrlich, S.; Krieg, H. A consistent and accurate ab initio parametrization of density functional dispersion correction (DFT-D) for the 94 elements H-Pu. *The Journal of chemical physics* **2010**, *132*, 154104.
(33) VandeVondele, J.; Hutter, J. Gaussian basis sets for accurate calculations on molecular systems in gas and condensed phases. *The Journal of chemical physics* **2007**, *127*, 114105.
(34) Lippert, B. G.; PARRINELLO, J. H.; MICHELE A hybrid Gaussian and plane wave density functional scheme. *Molecular Physics* **1997**, *92*, 477–488.
(35) VandeVondele, J.; Hutter, J. An efficient orbital transformation method for electronic structure calculations. *The Journal of chemical physics* **2003**, *118*, 4365–4369.
(36) Zhang, Y.; Wang, H.; Chen, W.; Zeng, J.; Zhang, L.; Wang, H.; E, W. DP-GEN: A concurrent learning platform for the generation of reliable deep learning based potential energy models. *Computer Physics Communications* **2020**, *253*, 107206.
(37) Zhang, L.; Han, J.; Wang, H.; Saidi, W.; Car, R.; E, W. End-to-end symmetry preserving inter-atomic potential energy model for finite and extended systems. *Advances in neural information processing systems* **2018**, *31*.
(38) Wang, H.; Zhang, L.; Han, J.; E, W. DeePMD-kit: A deep learning package for many-body potential energy representation and molecular dynamics. *Computer Physics Communications* **2018**, *228*, 178–184.
(39) Bussi, G.; Donadio, D.; Parrinello, M. Canonical sampling through velocity rescaling. *The Journal of chemical physics* **2007**, *126*.
(40) Barducci, A.; Bussi, G.; Parrinello, M. Well-tempered metadynamics: a smoothly converging and tunable free-energy method. *Physical review letters* **2008**, *100*, 020603.
(41) E, W. *Principles of multiscale modeling*; Cambridge University Press, 2011.
(42) Laio, A.; Parrinello, M. Escaping free-energy minima. *Proceedings of the national academy of sciences* **2002**, *99*, 12562–12566.
(43) Peter, C.; Oostenbrink, C.; Van Dorp, A.; Van Gunsteren, W. F. Estimating entropies from molecular dynamics simulations. *The Journal of chemical physics* **2004**, *120*, 2652–2661.
(44) Hansen, K. *Statistical physics of nanoparticles in the gas phase*; Springer, 2013.
(45) Li, S.; Liu, Y.; Sun, F.; Fang, H. Multi-particle molecular dynamics simulation: shell thickness effects on sintering process of Cu-Ag core-shell nanoparticles. *Journal of Nanoparticle Research* **2021**, *23*, 1–14.
(46) Liu, X.; Wen, X.; Hoffmann, R. Surface activation of transition metal nanoparticles for heterogeneous catalysis: what we can learn from molecular dynamics. *ACS Catalysis* **2018**, *8*, 3365–3375.
(47) Foster, D.; Pavloudis, T.; Kioseoglou, J.; Palmer, R. Atomic-resolution imaging of surface and core melting in individual size-selected Au nanoclusters on carbon. *Nature communications* **2019**, *10*, 2583.
(48) Vupputuri, S.; Tayebi, L.; Hikkaduwa Koralege, R. S.; Nigatu, A.; Mozafari, M.; Mishra, A.; Liu, L.; Ramsey, J. D. Polyethylene glycol–modified DOTAP: cholesterol/adenovirus hybrid vectors have improved transduction efficiency and reduced immunogenicity. *Journal of Nanoparticle Research* **2021**, *23*, 1–14.
(49) Matsuda, J.; Yamamoto, T.; Takahashi, S.; Nakanishi, H.; Sasaki, K.; Matsumura, S. In Situ TEM Investigation of Structural Changes in Ni Nanoparticle Catalysts under Gas Atmospheres: Implications for Catalyst Degradation. *ACS Applied Nano Materials* **2021**, *4*, 2175–2182.
(50) Yuan, W.; Zhu, B.; Fang, K.; Li, X.-Y.; Hansen, T. W.; Ou, Y.; Yang, H.; Wagner, J. B.; Gao, Y.; Wang, Y.; others In situ manipulation of the active Au-TiO2 interface with atomic precision during CO oxidation. *Science* **2021**, *371*, 517–521.
(51) Schlögl, R. Heterogeneous catalysis. *Angewandte Chemie International Edition* **2015**, *54*, 3465–3520.
(52) Xie, S.; Xu, Q.; Huang, X. Defect-Rich Metal Nanocrystals in Catalysis. *ChemCatChem* **2016**, *8*, 480–485.
(53) Yan, X.; Zhuang, L.; Zhu, Z.; Yao, X. Defect engineering and characterization of active sites for efficient electrocatalysis. *Nanoscale* **2021**, *13*, 3327–3345.
(54) Vendelbo, S. a.; Elkjær, C. F.; Falsig, H.; Puspitasari, I.; Dona, P.; Mele, L.; Morana, B.; Nelissen, B.; Van Rijn, R.; Creemer, J.; others Visualization of oscillatory behaviour of Pt nanoparticles catalysing CO oxidation. *Nature materials* **2014**, *13*, 884–890.
(55) Ghosh, T.; Arce-Ramos, J. M.; Li, W.-Q.; Yan, H.; Chee, S. W.; Genest, A.; Mirsaidov, U. Periodic structural changes in Pd nanoparticles during oscillatory CO oxidation reaction. *Nature Communications* **2022**, *13*, 6176.
(56) Lu, Y.; Yin, W.-J.; Peng, K.-L.; Wang, K.; Hu, Q.; Selloni, A.; Chen, F.-R.; Liu, L.-M.; Sui, M.-L. Self-hydrogenated shell promoting photocatalytic H2 evolution on anatase TiO2. *Nature communications* **2018**, *9*, 2752.
(57) Imaoka, T.; Yamamoto, K. Wet-chemical strategy for atom-precise metal cluster catalysts. *Bulletin of the Chemical Society of Japan* **2019**, *92*, 941–948.
(58) Han, M.; Xu, C.; Zhu, D.; Yang, L.; Zhang, J.; Chen, Y.; Ding, K.; Song, F.; Wang, G. Controllable Synthesis of Two-Dimensional Metal Nanoparticle Arrays with Oriented Size and Number Density Gradients. *Advanced Materials* **2007**, *19*, 2979–2983.

TOC Graphic